POLITECNICO DI TORINO
Repository ISTITUZIONALE

Quantitative assessment of rockfall-induced risks to infrastructure: a framework for fragmentation, mitigation measures and socioeconomic consequences

Original
Quantitative assessment of rockfall-induced risks to infrastructure: a framework for fragmentation, mitigation measures and socioeconomic consequences / Marchelli, M., De Biagi, V., Chiaia, B., Peila, D.. - ELETTRONICO. - (2026), pp. 1-8. (XV IAEG World Congress IAEG 2026 Engineering Geology in a Rapidly Changing World Delft (Nld) 30 October 2026-06 November 2026).

Availability:
This version is available at: 11583/3017615 since: 2026-11-06T10:33:50Z

Publisher:
IAEG 2026

Published
DOI:

Terms of use:

This article is made available under terms and conditions as specified in the corresponding bibliographic description in the repository

Publisher copyright

(Article begins on next page)

15 November 2026

https://dx.doi.org/xxxxx/xxxxx

Proceedings of the 15th IAEG World Congress IAEG 2026
Engineering Geology in a Rapidly Changing World
30 October to 6 November 2026
Delft University of Technology, The Netherlands

Quantitative assessment of rockfall-induced risks to infrastructure: a framework for fragmentation, mitigation measures and socioeconomic consequences

M. Marchelli[1,*], B. Chiaia[2], V. De Biagi[2], and D. Peila[1]

[1] Department of Environment, Land and Infrastructure Engineering (DIATI), Politecnico di Torino, C.so Duca degli Abruzzi, 24, 10129, Torino, Italy; maddalena.marchelli@polito.it, ORCID 0000-0002-9919-2916; daniele.peila@polito.it, ORCID 0000-0002-1771-8874
2 Department of Structural, Geotechnical and Building Engineering (DISEG), Politecnico di Torino, C.so Duca degli Abruzzi, 24, 10129, Torino, Italy; bernardino.chiaia@polito.it, ORCID 0000-0002-5469-2271; valerio.debiagi@polito.it , ORCID 0000-0003-1866-9362
*corresponding author

ABSTRACT

Accurately predicting the consequences of geohazards remains a major challenge in quantitative risk assessment. Public and private stakeholders often face difficulties in defining risk management strategies, prioritising interventions, and allocating resources for mitigation, particularly in the case of rockfall hazards, where ensuring resilient infrastructure and safe communities is increasingly urgent. Building on a quantitative risk assessment framework previously developed by the authors, this study presents an enhanced methodology that integrates a new fragmentation model for propagation analysis. Understanding the size and energy of blocks potentially impacting elements at risk is crucial for the accurate design of protective systems and the estimation of their probability of failure, enabling a more realistic assessment of residual risk. Consequences are analysed across both social and economic dimensions. By capturing the interplay between hazard dynamics, infrastructure vulnerability, and the effectiveness of protective measures, the proposed framework supports the development of safer and more resilient transport networks in rockfall-prone areas, and it serves as a robust decision-support tool for policymakers and public authorities. The method is applied to viable infrastructure exposed to rockfall, such as high-traffic or mountainous roads that often serve as the sole access routes to remote areas.

KEYWORDS: quantitative risk assessment, Fragmentation, Residual risk, Protective measures.

INTRODUCTION

Quantitatively assessing the risks posed by rockfall remains one of the most persistent challenges in engineering geology (Macciotta et al., 2020). Despite substantial advances in understanding detachment mechanisms, runout behaviour, and the performance of protective systems, predicting the consequences of rockfall events with sufficient precision for decision-making purposes continues to be difficult. This is especially true for transport infrastructure in mountainous terrain, where even relatively small events can lead to severe social and economic impacts, including casualties, prolonged road closures, and disruptions to essential services (Budetta et al., 2016; Ferlisi et al., 2012; Zhou et al., 2024). Because road networks often function as critical lifelines, individual rockfall events may trigger fatalities, extended closures, and large-scale interruptions to mobility and economic activity. Their vulnerability to natural hazards therefore calls for robust frameworks capable of integrating hazard intensity, structural response, and the broader consequences of network-level disruption.

Social risk, expressed as the annual probability of at least one fatality on a road section, depends on traffic volume, vehicle occupancy, the likelihood of closure, and the interaction between the probability of block arrival and the temporal presence of users. Economic risk extends beyond direct damage to include closure-induced travel delays, rerouting, shifts in exposure on alternative routes, and the potential amplification of social risk across the network (Rupi et al., 2015; Strada et al., 2015). More generally, risk formulations that explicitly couple the frequency–magnitude relationship of block releases with propagation, impact intensity, vulnerability, and exposure are essential.

Building on this foundation, a continuous, time-indexed approach to rockfall risk assessment has been introduced (Marchelli et al., 2025a), in which the expected loss over a selected horizon is obtained by integrating across all plausible release volumes and their

Published: dd/mm/yyyy
©2026 published by TU Delft OPEN Publishing on behalf of the authors under CC-BY-4.0 license

associated impact intensities. A specific adaptation for road networks has been developed, and the analytical procedures proposed by the Authors (Marchelli et al., 2022; Marchelli et al., 2025b) for viable mountain roads integrate these aspects by coupling closure probabilities with traffic redistribution models. This enables the assessment of both direct and indirect impacts, supporting decision-making and prioritisation at the network scale.

Once computed the risk and compared to the acceptability threshold, a crucial component to risk management is the design of mitigation measures, trajectory analyses remain indispensable to both stages, as they provide the impact intensity distributions entering the risk integral and the design actions required for sizing protective structures. However, standard trajectory models often overlook fragmentation, despite extensive experimental evidence showing that fragment size, energy, and dispersion direction vary systematically with impact velocity, discontinuity orientation and block geometry. Several laboratory and field tests, together with numerical models (Gili et al., 2022; Marchelli et al., 2025c) demonstrate that fragmentation markedly alters post-impact trajectories and thus the likelihood and severity of impacts along a slope or at an infrastructure location (Corominas et al., 2017; Lanfranconi et al., 2024). The implementation of fragmentation within probabilistic lumped-mass trajectory models has recently shown strong potential for improving predictions of runout, impact energies and barrier loadings, rendering trajectory analysis more representative of real-scale behaviour (Marchelli, 2026).

Within this context, the present study develops an integrated framework that, by merging continuous probabilistic risk quantification, network-level social and economic consequence analysis, and fragmentation-aware trajectory modelling, delivers more realistic hazard scenarios, traceable risk estimates, and evidence-based mitigation design for rockfall-prone transport infrastructure, demonstrated here through an Alpine case study that illustrates the full chain from hazard characterisation to protective measure sizing.

METHODOLOGY

Quantitative Risk Assessment Framework

The risk to an element at risk over a time horizon τ is expressed as the expected loss arising from all plausible release scenarios, their propagation patterns, impact intensities, vulnerability relationships, and exposure conditions. Following the general framework of Marchelli et al. (2025a), the risk is written as the expectation over release volumes and associated impact intensities:

$$R(\tau) = E(\tau)W \int_0^\infty \left[1 - e^{-\lambda(\tau)p_d(V_B)p_r^e(V_B)}\right]\left(\int_0^\infty \Psi(\psi, V_B) f_v(\psi|\, V_B) dv\right) dV_B \quad (1)$$

where $\lambda(\tau)$ is the time-dependent mean rate of block detachment; $p_d(V_B)$ denotes the probability density function of the release volume, which, combined with $\lambda(\tau)$, defines the volume–frequency relationship; $p_r^e(V_B)$ is the probability that a block of size V_B reaches the element; $f_v(\psi \mid V_B)$ is the distribution of impact intensity (typically velocity v or derived energy) conditional on volume; $\Psi(\psi, V_B)$ is the vulnerability function (loss ratio); $E(\tau)$ is exposure, i.e., the time-dependent probability that the element is present when an impact occurs; and W is the element's value under the adopted loss metric. This formulation requires a double integration: first over all admissible impact intensities for each block size, and then over all admissible release volumes. For rare events, a McLaurin expansion yields the first-order approximation:

$$R(\tau) \approx E(\tau)\, W \int_0^\infty [\lambda(\tau)p_d(V_B)p_r^e(V_B)]\left(\int_0^\infty \Psi(\psi, V_B) f_v(\psi|\, V_B) dv\right) dV_B \quad (2)$$

where data are sparse, a discrete/binned implementation is preferred, replacing the integrals with finite sums while preserving the multi-scenario logic.

Social risk quantification for road network

When focusing on road infrastructure and on people travelling within vehicles as elements at risk, and when block-arrival rates at the carriageway are available (e.g., from event logs or sensor data), the annual probability that at least one block reaches a given road segment is $P_{S:T}(1\text{y})$, while $\lambda_r(1\text{y})$ is the mean number of blocks reaching that segment per year.

Within a probabilistic framework consistent with Eq. (1), social damage, and thus social risk, is quantified as the probability of incurring at least one victim. This is computed through an event-tree that considers three mutually exclusive fatality-related scenarios: (i) impact of a moving vehicle by an incoming block, (ii) collision of a vehicle with a stationary block lying on the carriageway, and (iii) loss of vehicle control due to pavement damage caused by block impact. The framework evaluates the

probability that a vehicle is within the impact footprint at block arrival, the probability that a vehicle is unable to stop in time when encountering a stationary block or damaged pavement, and the lethality associated with each scenario. Road geometry, curvature, sight distance, stopping visibility, and expected traffic conditions (annual flow and speed distributions) are essential inputs to estimate the fatality probability conditional on at least one block reaching the road, denoted P_{victim}.

The annual social risk for a road segment is thus:

$$R_{1y} = 1 - e^{-\lambda_r (1y)\, P_{\text{victim}}}. \tag{3}$$

When multiple roads connect two points, closure of one link alters the traffic loads and exposure on the remaining open routes. Consequently, social risk at network scale must reflect (i) the closure probability of each road, (ii) the redistribution of traffic during closure periods, (iii) the increased exposure and therefore higher social risk on alternative routes.

The extended formulation of network social risk R_{sN}^{c} (with closures) follows the multi-scenario expansion, accounting for combinations of closures of one or more roads:

$$R_{sN}^{c} \cong \underbrace{R_{sN}(1y) \prod_{r_i=1}^{N} \left(1 - P_{(S:T)_{r_i}}\right)}_{(A)} + \sum_{r_i=1}^{N} \underbrace{P_{(S:T)_{r_i}} \prod_{r_j=1}^{N-1} \left(1 - P_{(S:T)_{r_j \neq i}}\right) \left[R_{sN}(1y - \tau_i) + R_{sN}^{new}(\tau_i)\right]}_{(B_i)} + \Omega, \tag{4}$$

being $R_{sN}(1y)$ the social risk of the intact network (no closure), computed as the sum of the risk for each of the N roads $R_{s_{r_i}}(1y)$, and $R_{sN}^{new}(\tau_i)$ the risk of the network during the closure of road i, given by the sum of the risk for each remaining open road, considering the increase in traffic. The term $R_{sN}(1y - \tau_i)$ represents the risk of the network computed for the period in which no closures are applied. The term $P_{(S:T)_{r_i}}$ is the annual probability that at least one block road i. The term (A) represents contribution to network risk when no road is closed, where $\left(1 - P_{(S:T)_{r_i}}\right)$ is the probability of no closure on road i, and the product $\prod_{r_i=1}^{N} \left(1 - P_{(S:T)_{r_i}}\right)$ running over all roads gives the joint probability that no road is simultaneously closed; while the term (B_i) is the risk of alternately closing roads, while the term Ω accounts for closures of couples of roads during the same year. For very small event probabilities, the simplified expression becomes:

$$R_{sN}^{c} = R_{sN}(1y) \left(1 - \sum\nolimits_{r_i=1}^{N} P_{(S:T)_{r_i}}\right) + \sum_{r_i=1}^{N} P_{(S:T)_{r_i}} \left(R_{sN}(1y - \tau_i) + R_{sN}^{new}(\tau_i)\right). \tag{5}$$

Economic risk quantification for road network

Similarly, economic risk accounts for both direct and indirect costs induced by road closures following block impacts. Let:

$$\Delta C_{r_i} = C_{r_i} - C_0$$

be the variation in total travel cost (generalized cost × traffic volume) when road i is closed, relative to the baseline condition $C_0$where all roads are operative, computed as the product of the value of travel time, the mean trip length, and the annual traffic volume under normal network conditions. The generalised travel cost C_{r_i} represents the total cost borne by network users when road i is closed, computed as the product of the additional travel time per trip, the value of travel time, and the annual traffic volume redistributed onto alternative routes; it is conveniently expressed in minutes of additional travel per year accumulated across all network users, providing an intuitive metric for ranking closure scenarios and prioritising interventions. Repair costs for road i are denoted as C_{rep,r_i}, i.e. the direct reinstatement cost following a damaging rockfall event on road i (including cleanup, barrier repair, and surface reinstatement). Neglecting closures of more than two roads within the same year (due to the very low joint probability), the annual economic risk of the network is:

$$R_{eN}^{c} = \sum_{r_i=1}^{N} P_{S:T,r_i} \prod_{r_j \neq r_i} (1 - P_{(S:T)_{r_j}}) \left(\Delta C_{r_i} + C_{\text{rep},r_i}\right) + \sum\nolimits_{r_i, r_j} P_{S:T,r_i} P_{S:T,r_j} \prod\nolimits_{r_k \neq i,j} (1 - P_{(S:T)_{r_k}}) \left(\Delta C_{r_i} + C_{rep,r_i} + \Delta C_{r_j} + C_{rep,r_j}\right). \tag{6}$$

For very small closure probabilities, the formulation simplifies into:

$$R_{eN}^{c} \approx \sum_{r_i=1}^{N} P_{S:T,r_i} \left(\Delta C_{r_i} + C_{\mathrm{rep},r_i}\right), \tag{7}$$

which allows identifying the economically most critical road segments by comparing the cost consequences of their individual closures.

Mitigation Design and Fragmentation-Aware Trajectory Modelling

Once the risk has been quantified and compared with acceptability thresholds, trajectory analyses remain indispensable to both stages: they provide the impact intensity distributions (in terms of block or fragment mass and velocity, and hence kinetic energy and impact height) entering the risk integral and the design actions required for sizing protective structures. In accordance with UNI 11211-4:2018, characteristic design actions are defined as the 95th percentiles of impact energy and impact height at the mitigation line, multiplied by the corresponding partial safety factors, requiring the selection of a representative block volume from field evidence or conservatively from the upper tail of the block-size distribution. However, standard trajectory models frequently overlook fragmentation, despite extensive field and laboratory evidence demonstrating that fragment size, energy and dispersion direction vary systematically with impact velocity, block shape, internal structure and discontinuity orientation (Matas et al., 2020; Gili et al., 2022). Models treating blocks as intact bodies cannot capture these effects reliably, and predictions of arrival probability, impact intensities and load cases at the mitigation line may be significantly misrepresented if fragmentation is ignored. Fragmentation-aware trajectory modelling is therefore indispensable for reliable mitigation design.

In the present study, mitigation design is supported through RockFRAG (Marchelli, 2026), a probabilistic lumped-mass trajectory model that explicitly incorporates fragmentation at each impact. The trajectory engine treats each block-surface interaction as a coupled contact-fracture event. Fragmentation is triggered whenever the normal component of translational kinetic energy at impact exceeds a threshold $E_{th} = \widetilde{\sigma_t}^{5/3} Y_{eq}^{-\frac{2}{3}} d_{eq}^3 k_{s,th}$, where $\widetilde{\sigma_t}$ is the effective tensile strength (accounting for rock mass quality and joint orientation at the impact, with joint orientation sampled probabilistically via Monte Carlo at each contact), Y_{eq} the Hertzian contact deformation coefficient, d_{eq} the equivalent block diameter, and $k_{s,th}$ a shape factor (2.0 for cube, 1.7 for slab-like, 1.5 for prismatic blocks). The threshold and its correction factors were calibrated on laboratory drop tests on intact and jointed specimens (Marchelli et al., 2025c, and see Marchelli, 2026 for details). When breakage occurs, fragment masses are sampled from a bilinear log-log complementary cumulative distribution characterised by a fixed lower bound, i.e. minimum fragment = 0.1% of parent mass, the slopes of the two linear segments and the location of their transition point depend on both rock-mass condition and the energy ratio between the normal translational kinetic energy at the impact and the E_{th}, through exponential fitting expressions calibrated on drop tests on jointed spherical specimens (Marchelli et al., 2025c). Sampling proceeds iteratively enforcing mass conservation until the cumulative fragment mass equals the parent block mass; fragments below the minimum threshold mass are discarded. Each fragment is then assigned post-impact velocity components through an effective restitution coefficient COR*, sampled from condition- and orientation-dependent statistical distributions and scaled to the specific mechanical properties of the impacted surface, and a launch angle α sampled within experimentally observed bounds. Each generated fragment is propagated as an independent block subject to the same contact-fracture logic; it inherits the mechanical properties and rock-mass structural condition of the parent block, except for fragments generated from moderately fractured blocks whose volume falls below a user-defined threshold, which are reclassified as intact for all subsequent impacts, thus enabling recursive simulation of multi-impact fragmentation chains. Preliminary model validation and sensitivity analyses, covering fragmentation probability, fragment-size statistics, runout envelopes and shape-dependent propagation, are reported in Marchelli (2026). The model thus generates complete runout envelopes, arrival probabilities, and distributions of impact energy and height at any user-defined control section, directly populating the reach probability $p_r^e(V_B)$ and the conditional intensity distribution $f_v(\psi \mid V_B)$ that enter the risk integral.

By embedding a physically informed and experimentally calibrated fragmentation module within a probabilistic trajectory model, the proposed approach provides mitigation designers with evidence-based impact scenarios, enabling more accurate residual risk assessment and more robust prioritisation among protective options.

EXAMPLE OF APPLICATION

The application refers to a mountain site in the Northwestern Italian Alps. The area is crossed by two roads (#1 and #2), the latter represents the only access to several hamlets distributed on the slope. The geological and geomorphological framework of the area is complex and inherently predisposed to gravitational instability. The slope belongs to the Sesia–Lanzo Zone of the Austroalpine Domain and is mainly composed of Gneiss Minuti with a pervasive schistosity, cut locally by lamprophyre dykes. The rock mass is overlain by extensive colluvial and detrital mantles, and the presence of a documented Deep-Seated Gravitational Slope Deformation

(DGPV) further contributes to widespread fracturing, tensile cracks, and localised settlement features. The forest cover, dominated by chestnut stands in the lower elevations and beech higher upslope, only partially mitigates rockfall propagation, as past events have shown that larger blocks easily break through the vegetation and reach the roads. Multiple historical rockfalls (1993–2024) confirm an active and persistent process operating over the entire slope, with impacts recorded repeatedly on both infrastructures. A detailed topographic survey enabled the identification of the main potential source zones, supporting the delineation of sectors with recurrent instability and guiding the selection of representative release areas for the propagation analyses (Figure 1).

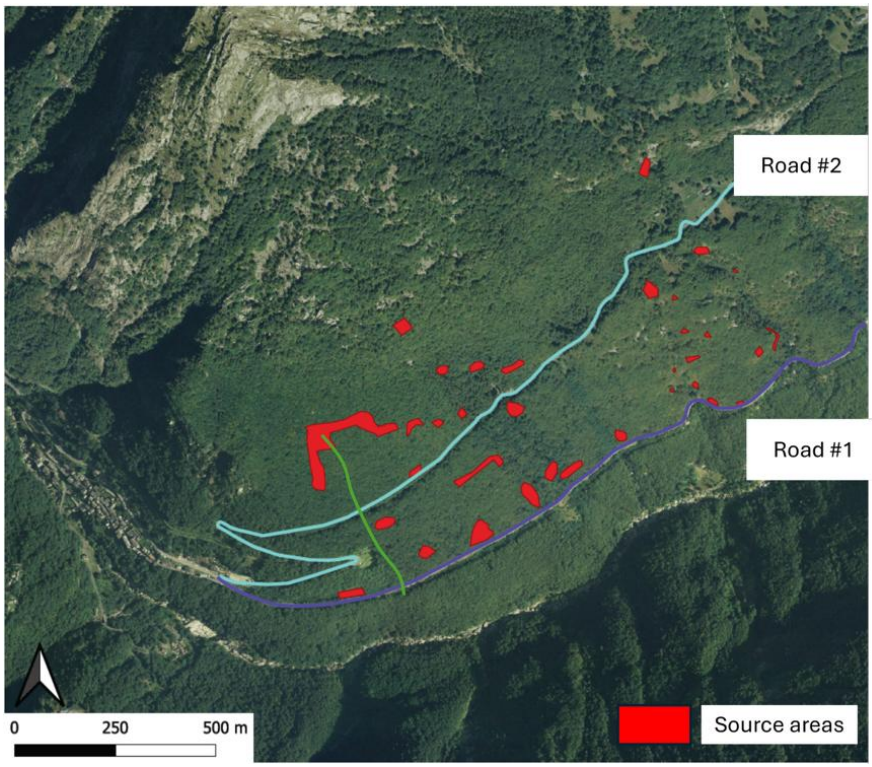


Figure 1: Overview of the study area. The two analysed roads are shown in blue (Road #1) and light blue (Road #2). Source areas are highlighted in red. The green lines indicate the 2D cross-sections used for the design of the rockfall protection barriers.

Social and economic risk quantification

To quantify the social and economic consequences of rockfall on these roads, the annual arrival frequency was assumed equal to the annual detachment frequency, $\lambda_r(1\text{y}) = 0.5$, consistent with the recurrence of events recorded in the regional landslide cadastre and with several significant detachments documented in the past three decades. Vehicle speeds average 50 km/h on Road #1 and 40 km/h on Road #2, with mean hourly flows of 30 and 10 vehicles per hour, respectively. These values enter the event-tree formulation, enabling the computation of social risk for moving vehicles, resulting in $R_{sN}(1y)$ equal to $2.77 \cdot 10^{-7}$ and $3.47 \cdot 10^{-7}$ for Road #1 and Road #2, respectively. For the economic risk, only travel-time increments are considered. Repair costs C_{rep,r_i} are neglected for simplicity. A closure duration of one month is assumed for reparation works following a damaging event, consistent with typical intervention times for rockfall clean-up, barrier repair and surface reinstatement in similar Alpine settings. Under the assumption that the closure of a road results in a 10% increase in travel time per passage, the associated increments in generalised travel cost were computed for all closure combinations. These outputs, together with the network social-risk results, are summarised in Table 1. The road network configuration, composed of two interdependent routes with no viable alternatives, results in a cumulative annual social risk of the order of 10^{-5} and an annual economic risk corresponding to approximately 16.7 minutes of expected delay, indicating a non-negligible impact at network scale. In particular, the social-risk contribution is of similar magnitude across the four scenarios, with values of the order of 10^{-6}, reflecting the relatively the moderate traffic volumes on both roads, while the economic-risk component shows stronger variation. Closure of Road #1 contributes the largest share (7.7 min of expected annual travel-time increase), consistent with its higher traffic demand and its role as the principal access route to the valley. Closure of the Road #2 alone produces only 0.7 min of annual expected delay. When both roads are closed, whether due to simultaneous events or as a consequence of cascading operational constraints, the total expected increase in annual travel time reaches 8.3 min highlighting the critical role of Road #1 in maintaining efficient and reliable access to the hamlets.

191 **Table 1. $R_{sN}(1y)^c$ and $R_{eN}(1y)^c$ in different conditions**

	No closure	*Closure Road #1*	*Closure Road #2*	*Both closures*
R_{sN}^c *(-)*	*2.95E-06 (A in Eq. (4))*	*2.99E-06 (B_1 in Eq. (4))*	*2.93E-06 (B_2 in Eq. (4))*	*2.98E-06 (Ω in Eq. (4))*
		Total: 1.18E-05		
ΔC_{r_i} *(min)*	-	*30.7*	*2.7*	*33.4*
R_{eN}^c *(min)*	-	*7.7*	*0.7*	*8.3*
		Total: 16.7		

192 Mitigation measure design

193 For the design of mitigation measures, the first step consists in identifying an appropriate block volume for detailed propagation
194 analyses. Following the principles of UNI 11211-4:2018, a representative initial volume of 10 m³ was selected. This value
195 corresponds approximately to the 99th percentile of the observed block-size distribution, accounting for unitary rock volumes (VRU)
196 in the rock face documented in several past events and providing a conservative estimate of the potential block reaching the roads.
197 Using λ_r = 0.5 yr^{-1}, such a block has an implicit return period of roughly 200 years, representing an extreme but physically plausible
198 scenario for which protective measures must guarantee performance. Before conducting detailed trajectory modelling, the block–
199 soil interaction parameters were calibrated through back-analyses of the events of 2010, 2012 and 2024, which provided reliable
200 observations of impact positions and arrest locations at different points along well-mapped trajectories. These analyses ensured that
201 the restitution coefficients (normal R_n and tangential R_t sliding friction angle ϕ, and the influence of vegetation were correctly
202 represented in the simulations. In particular, the calibrated restitution coefficients fell within $R_n = 0.5 \pm 0.12$ and $R_t = 0.9 \pm 0.1$ for
203 asphalt, and $R_n = 0.4 \pm 0.12$ and $R_t = 0.8 \pm 0.12$ for the remaining portions of the slope affected by soil, debris and vegetation,
204 where ± denotes one standard deviation from back-analysis, consistent with the Monte Carlo sampling approach. A friction angle
205 of φ ≈ 20°±1 was adopted to consistently reflect the lumped-mass assumption, where pure rolling is not explicitly modelled to
206 reproduce the observed behaviour. For the fragmentation module, a spherical block shape was assumed as a representative and
207 conservative geometric configuration, ensuring cautelative estimates of impact energies, rebound heights and runout distances.
208 Subsequently, 2D trajectory analyses were performed along a series of cross-sections specifically chosen to intersect the most
209 probable paths identified in the 3D propagation modelling and field inspections. Each section was analysed both without
210 fragmentation (intact 10 m³ block) and with fragmentation. The fragmentation threshold E_{th} was evaluated considering a tensile
211 strength of the block material of 5.0± 0.7 MPa and a Young modulus of 30± 3 GPa, consistent with intact gneissic rock. As
212 mentioned in the methodology, the fragmentation model applied a bilinear complementary cumulative distribution to compute
213 fragment sizes with the slopes of the two linear segments and their transition point were computed from exponential functions of
214 the energy ratio and rock mass condition, identified as competent for this site, while post-impact fragment kinematics were assigned
215 through an effective restitution coefficient COR* sampled from a Uniform(0.16, 0.31) distribution, consistent with the same rock
216 mass conditions (Marchelli, 2026). Table 2 summarises the worst 95th-percentile values of impact velocity v_{95}, kinetic energy
217 $E_{k,95}$ and impact height h_{95} obtained from the detailed 2D trajectory simulations, both with and without fragmentation. For Road
218 #1, the most severe values originate from source areas located above Road #2, where the greater vertical drop enables blocks to
219 maintain high energies in the intact-block scenario and to reach the regional road with substantial rebound heights when
220 fragmentation is considered. In the non-fragmentation case, simulations show that the great majority of blocks released from upper
221 source areas (often more than 80%) stop directly on Road #2, and only the remaining fraction continues downslope towards Road
222 #1 with few or no intermediate stops, following compact and predictable trajectories (Figure 2: Empirical cumulative density
223 function of the stopping point, for the two simulations (without and with fragmentation).Figure 2). When fragmentation is included,
224 however, the behaviour changes significantly: blocks impacting Road #2 tend to break, generating fragments that retain enough
225 mobility to continue their runout and eventually reach Road #1, where they arrive with lower energy but markedly higher rebound
226 heights. For Road #2, fragmentation produces the same trend but with a more moderate effect: the 95th-percentile kinetic energy
227 decreases while the impact height moderately increases going from the without- to the with-fragmentation scenario. This illustrates
228 how analyses neglecting fragmentation may underestimate the likelihood of block propagation beyond intermediate roads and, more
229 critically, may fail to capture the increased overpassing potential due to higher bounce heights. These findings indicate that, in the
230 absence of mitigation, both infrastructures remain exposed to high-energy events, particularly during intense rainfall episodes when
231 detachment probability increases. A feasible risk-reduction strategy may include either temporary road closures during rainfall
232 periods or the installation of a double line of rockfall protection barriers; considering the performance levels of commercially
233 available certified systems, the lower barrier should feature a maximum energy level (MEL) of at least 8,000 kJ and a height of 7

m, ensuring interception of both intact blocks and high-bounce fragments, while the upper barrier, intercepting blocks before they reach Road #2, could be sized for a lower energy level consistent with the reduced intensities observed at that location.

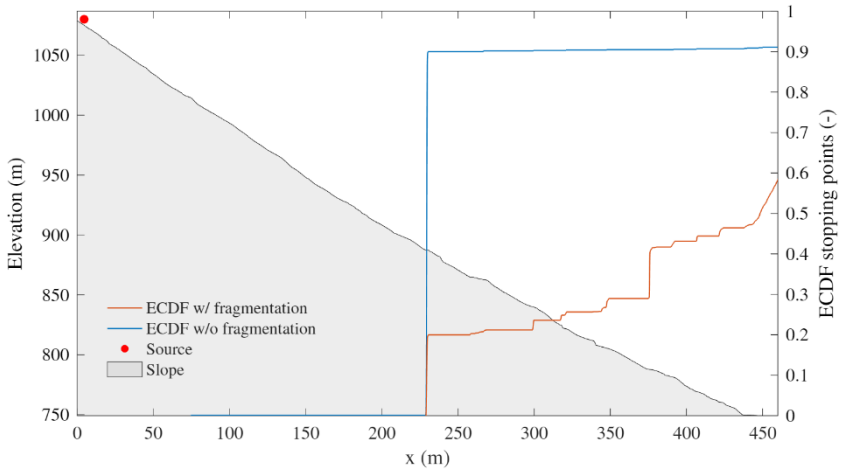


Figure 2: Empirical cumulative density function of the stopping point, for the two simulations (without and with fragmentation).

Table 2. 95th percentile kinetic energy and impact height

Road	*Scenario*	$v_{95}(m/s)$	$E_{k,95}\ (kJ)$	$h_{95}\ (m)$
Road #1	*Without fragmentation*	*38*	*19494*	*7*
Road #1	*With fragmentation*	*35*	*10000*	*15*
Road #2	*Without fragmentation*	*21*	*5953*	*0.5*
Road #2	*With fragmentation*	*22*	*2300*	*1.7*

CONCLUSION

This study presents an integrated framework for quantitatively assessing rockfall risk to infrastructure, combining continuous probabilistic formulations with network-scale social and economic consequence models. By explicitly incorporating fragmentation within trajectory simulations, the method overcomes key limitations of traditional propagation tools and provides more realistic size-energy-height spectra for mitigation design. The proposed approach strengthens the link between hazard characterization, infrastructure vulnerability, and the effectiveness of protective systems, enabling a more accurate estimation of both direct and indirect impacts. Its formulation supports decision-makers in prioritising interventions, managing residual risk, and identifying the most critical elements within transport networks. Although demonstrated here through a specific Alpine application, the framework is fully general and can be implemented in a wide range of geomorphological and infrastructural settings. Overall, the results highlight the importance of combining probabilistic risk modelling, fragmentation-aware trajectory analysis, and network-level consequence assessments to design robust mitigation solutions and enhance the resilience of road infrastructures exposed to rockfall hazards.

ACKNOWLEDGEMENTS

This work was supported by Marie Curie Postdoctoral Fellowship 2022 (Call Horizon-MSCA-2022-PF-01, grant GA101103401 - RIDETHERISK project) and by the PNRR NODES project''Nord Ovest Digitale E Sostenibile'', funded by the MUR—M4C2 1.5 of PNRR program (n◦ ECS00000036).

CONTRIBUTION STATEMENT

Conceptualization (M.M.); Data Curation (M.M., V.D.B.); Analysis (M.M.); Investigation (M.M.); Methodology (M.M, V.D.B.); Writing (M.M.); Funding acquisition (M.M.); Writing - Review & Editing (all).

REFERENCES

Budetta, P. D. L. C., De Luca, C., & Nappi, M. (2016). Quantitative rockfall risk assessment for an important road by means of the rockfall risk management (RO. MA.) method. *Bulletin of Engineering Geology and the Environment*, *75*(4), 1377-1397.

Corominas, J., Matas, G., & Ruiz-Carulla, R. (2019). Quantitative analysis of risk from fragmental rockfalls. *Landslides*, *16*(1), 5-21.

Ferlisi, S., Cascini, L., Corominas, J., & Matano, F. (2012). Rockfall risk assessment to persons travelling in vehicles along a road: the case study of the Amalfi coastal road (southern Italy). *Natural hazards*, *62*(2), 691-721.

Gili, J. A., Ruiz-Carulla, R., Matas, G., Moya, J., Prades, A., Corominas, J., ... & Mavrouli, O. (2022). Rockfalls: analysis of the block fragmentation through field experiments. *Landslides*, *19*(5), 1009-1029.

Lanfranconi, C., Frattini, P., Agliardi, F., Stock, G. M., Collins, B. D., & Crosta, G. (2024). Field evidence and indicators of rockfall fragmentation and implications for mobility. *Engineering Geology*, *341*, 107704.

Macciotta, R., Gräpel, C., Keegan, T., Duxbury, J., & Skirrow, R. (2020). Quantitative risk assessment of rock slope instabilities that threaten a highway near Canmore, Alberta, Canada: managing risk calculation uncertainty in practice. *Canadian Geotechnical Journal*, *57*(3), 337-353.

Matas, G., Lantada, N., Corominas, J., Gili, J., Ruiz-Carulla, R., & Prades, A. (2020). Simulation of full-scale rockfall tests with a fragmentation model. *Geosciences*, *10*(5), 168.

Marchelli, M., De Biagi, V., Bertolo, D., Paganone, M., & Peila, D. (2022). A mixed quantitative approach to evaluate rockfall risk and the maximum allowable traffic on road infrastructure. Georisk: Assessment and Management of Risk for Engineered Systems and Geohazards, 16(3), 584-594.

Marchelli, M., De Biagi, V., & Chiaia, B. (2025a). A fully probabilistic framework to compute the residual rockfall risk in presence of mitigation measures. Landslides, 22(9), 2961-2968.

Marchelli, M., Peila, D., & Chiaia, B. (2025b). Quantitative risk assessment for viable infrastructures subjected to rockfall: analyses of social and economical consequences. In proceedings of the 9th International Symposium for Geotechnical Safety and Risk ISGSR 2025, pp. 1-4.

Marchelli, M., Guccione, D. E., Giacomini, A., & Buzzi, O. (2025c). Fragmentation Patterns and Trajectories During Rockfall: Analysis of the Influence of Discontinuities and Impact Conditions Through Drop Tests: M. Marchelli et al. *Rock Mechanics and Rock Engineering*, 1-33.

Marchelli, M. (2026). A new probabilistic rockfall trajectory model incorporating fragmentation, rock mass quality and block shape variability. *International Journal of Rock Mechanics and Mining Sciences,* 206,106624.

Rupi, F., Bernardi, S., Rossi, G., & Danesi, A. (2015). The evaluation of road network vulnerability in mountainous areas: a case study. *Networks and Spatial Economics*, *15*(2), 397-411.

Strada, C., Tagnin, S., Mottironi, M., Larcher, V., Villa, G., & Mair, V. (2015). Management of Rock Fall Risk on the Main Roads of Southtirol. In *Engineering Geology for Society and Territory-Volume 2: Landslide Processes* (pp. 1829-1833). Cham: Springer International Publishing.

UNI 11211-4 (2018). Opere di difesa dalla caduta massi - Parte 4: Progetto definitivo ed esecutivo. UNI Ente Italiano di Normazione

Zhou, S., Huang, Y., Guo, Z., & Ouyang, C. (2024). Quantitative risk assessment of road exposed to landslide: A novel framework combining numerical modeling and complex network theory. *Engineering Geology*, *343*, 107794.